Two Novel One-dimensional Inorganic-Organic Hybrids Constructed from $[H_2W_{12}O_{40}]^{6-}$ Clusters and Lanthanide-organic Complexes: $[(C_5H_5N\text{-}CO_2)_2\mathit{Ln}(H_2O)_3]_2[H_2W_{12}O_{40}]\cdot n H_2O$ ($C_5H_5N\text{-}CO_2$ = Pyridine-4-carboxylate; $\mathit{Ln} = La^{3+}$, $n = 5$; Ce^{3+}, $n = 7$)

Hai-jun Pang, Ya-guang Chen, Fan-xia Meng, and Dong-mei Shi

Key Laboratory of Polyoxometalates Science of the Ministry of Education, College of Chemistry, Northeast Normal University, Changchun 130024, P. R. China

Reprint requests to Dr. Yaguang Chen. E-mail: chenyg146@nenu.edu.cn

Z. Naturforsch. **2008**, *63b,* 16 – 22; received August 15, 2007

Two novel polyoxotungstate-based rare earth compounds, $[(C_5H_5N\text{-}CO_2)_2\mathit{Ln}(H_2O)_3]_2$-$[H_2W_{12}O_{40}] \cdot nH_2O$ ($C_5H_5N\text{-}CO_2$ = pyridine-4-carboxylate; $\mathit{Ln} = La^{3+}$ (**1**), $n = 5$; Ce^{3+} (**2**), $n = 7$), have been synthesized in aqueous solution and characterized by single-crystal X-ray diffraction, elemental analyses, IR spectra and TG analyses. The isostructural compounds **1** and **2** exhibit one-dimensional (1D) zig-zag chains, in which the dinuclear lanthanide complexes act as bridging linkers and the $[H_2W_{12}O_{40}]^{6-}$ groups serve as bidentate ligands. The results of cyclic voltammetry (CV) show that compounds **1** and **2** undergo two two-electron redox processes, similar to that of the parent $(NH_4)_6[H_2W_{12}O_{40}] \cdot 3H_2O$, and also reveal that the pH of the supporting electrolytic solution has a notable effect on the electrochemical behavior of compound **2**.

Key words: Polyoxometalates, Lanthanide, Electrochemical Properties

Introduction

Polyoxometalates (POMs), as early transition metal oxide clusters, have attracted extensive interest in fields such as catalysis, medicine, and materials science [1 – 6]. By using POMs as inorganic building blocks, a large number of POMs modified by metal complexes have been found since the first such modified α-Keggin POMs were reported by Xu *et al.* [7]. Zubieta [8], Pope [9], Gutierrez-Zorrilla [10], Long [11] and Wang and their co-workers [12 – 14] already have synthesized several hybrid materials with attractive structures and properties. However, with regard to POM-based hybrids, the rational synthesis of rare earth complex-modified POMs remains a challenge [15 – 17]. The reason is that oxygen atoms on the surface of POMs are rather reactive and easily combine with the highly oxophilic rare earth ions to form precipitates instead of crystals. So, recently, the introduction of protecting organic ligands, whose coordination to rare earth ions can decrease the highly oxophilic properties of the latter, could be used as one effective method to inhibit precipitation [18, 19]. Compared with the commonly used POMs, such as Keggin- [20], Wells-Dawson- [21], Anderson- [22] and paradodecametalate-B-type POMs [23], the α-metatungstate anion $[H_2W_{12}O_{40}]^{6-}$ has been less employed previously [24].

In order to obtain rare earth complexes of the α-metatungstate anion $[H_2W_{12}O_{40}]^{6-}$, we chose pyridine-4-carboxylic acid as the protecting organic ligand, and the rare earth ions La^{3+} and Ce^{3+} as the linkers to synthesize hybrids with extended structures by conventional methods. Herein, we report on two novel 1D zig-zag chainlike compounds $[(C_5H_5N\text{-}CO_2)_2\mathit{Ln}(H_2O)_3]_2[H_2W_{12}O_{40}]\cdot nH_2O$ ($C_5H_5N\text{-}CO_2$ = pyridine-4-carboxylate; $\mathit{Ln} = La^{3+}$ (**1**), $n = 5$; Ce^{3+} (**2**), $n = 7$). To the best of our knowledge, compounds **1** and **2** are the first examples of 1D structures consisting of $[H_2W_{12}O_{40}]^{6-}$ clusters, lanthanide cations and organic anions.

Results and Discussion

Description of the structures

The structures of **1** and **2** are all built up from α-metatungstate polyanions $[H_2W_{12}O_{40}]^{6-}$, Ln^{3+} cations and pyridine-4-carboxylate anions. The

0932–0776 / 08 / 0100–0016 $ 06.00

Table 1. Selected bond lengths (Å) and angles (°) for **1** and **2**[a].

	Distances (Å)			Angles (deg)	
	Ln = La (**1**)	*Ln* = Ce (**2**)		*Ln* = La (**1**)	*Ln* = Ce (**2**)
Ln(1)–OW1	2.572(9)	2.501(10)	O(7)–*Ln*(1)–O(41)	80.5(3)	80.8(3)
Ln(1)–OW2	2.523(10)	2.547(10)	O(7)–*Ln*(1)–O(42)$^{**\sharp}$	117.3(3)	118.1(3)
Ln(1)–OW3	2.487(10)	2.501(10)	O(7)–*Ln*(1)–O(43)	124.2(3)	123.7(3)
Ln(1)–O(7)	2.495(8)	2.479(9)	O(7)–*Ln*(1)–O(44)$^{**\sharp}$	67.9(3)	68.1(3)
Ln(1)–O(41)	2.535(9)	2.501(10)	O(9)–*Ln*(2)–O(45)	125.6(3)	125.7(4)
Ln(1)–O(43)	2.514(10)	2.502(10)	O(9)–*Ln*(2)–O(47)	116.4(3)	116.0(3)
Ln(1)–O(41)**	2.711(9)	2.511(11)	O(9)–*Ln*(2)–O(48)	80.8(3)	80.5(3)
Ln(1)–O(42)$^{**\sharp}$	2.627(9)	2.612(10)	O(41)–*Ln*(1)–O(41)**	78.9(3)	78.4(4)
Ln(1)–O(44)$^{**\sharp}$	2.517(11)	2.501(10)	O(41)–*Ln*(1)–O(42)$^{**\sharp}$	120.3(3)	120.1(3)
Ln(2)–OW4	2.554(9)	2.545(10)	O(43)–*Ln*(1)–O(41)	69.4(3)	69.5(3)
Ln(2)–OW5	2.518(10)	2.504(11)	O(43)–*Ln*(1)–O(42)$^{**\sharp}$	118.4(3)	118.2(3)
Ln(2)–OW6	2.501(9)	2.469(11)	O(43)–*Ln*(1)–O(44)	135.1(3)	136.0(4)
Ln(2)–O(9)	2.507(9)	2.490(11)	O(44)$^{**\sharp}$–*Ln*(1)–O(41)	71.2(3)	71.7(4)
Ln(2)–O(45)	2.508(9)	2.494(10)	O(44)$^{**\sharp}$–*Ln*(1)–O(42)$^{**\sharp}$	66.4(3)	66.5(3)
Ln(2)–O(47)	2.603(9)	2.591(10)	O(45)–*Ln*(2)–O(46)	70.0(3)	69.8(3)
Ln(2)–O(48)	2.730(9)	2.732(10)	O(45)–*Ln*(2)–O(47)$^{\sharp\sharp}$	118.0(3)	118.3(4)
Ln(2)–O(46)$^{*\sharp\sharp}$	2.514(9)	2.491(10)	O(45)–*Ln*(2)–O(48)	135.8(3)	136.0(4)
Ln(2)–O(48)*	2.530(10)	2.522(9)	O(46)$^{*\sharp\sharp}$–*Ln*(2)–O(47)	67.6(3)	66.9(4)

[a] Symmetry codes for **1**: * $-x+1$, $-y-2$, $-z+2$; ** $-x+1$, $-y$, $-z+1$; for **2**: $^{\sharp}$ $-x-1$, $-y+2$, $-z$; $^{\sharp\sharp}$ $-x-1$, $-y$, $-z+1$.

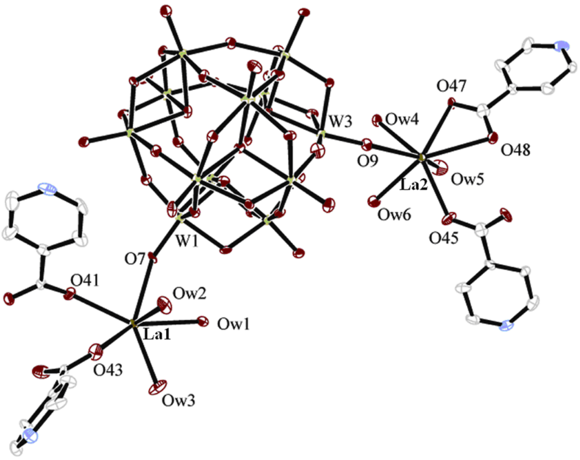

Fig. 1. ORTEP drawing of **1** with thermal ellipsoids set at 50 % probability; C gray, N light blue, O red, La dark blue and W green. Hydrogen atoms and water solvate molecules are omitted for clarity (color online).

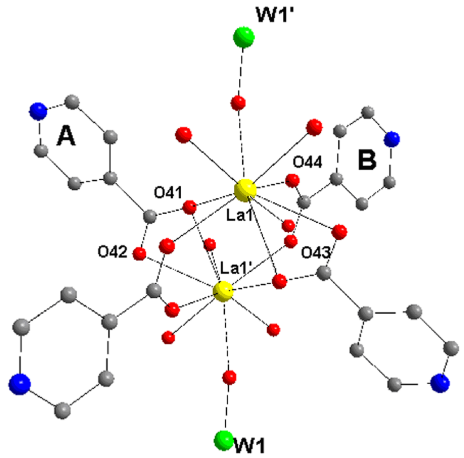

Fig. 2. The structure of the dimeric La1 coordination unit $\{(C_6H_5NO_2)_2La1(H_2O)_3\}_2$ in **1**. Hydrogen atoms omitted for clarity.

$[H_2W_{12}O_{40}]^{6-}$ cluster has a classic α-Keggin structure described previously, which can be viewed as the usual arrangement of four W_3O_{13} groups, each of which consists of three edge-sharing WO_6 octahedra. According to their different coordination environments in the polyanion, the oxygen atoms can be divided into four groups: terminal oxygen atoms, Ot; terminal oxygen atoms linked to Ln^{3+}, Ot′; bridging oxygen atoms, Ob; and central oxygen atoms Oc.

Single-crystal structural analyses reveal that compounds **1** and **2** are isomorphous, and therefore, the structure of **1** is described here representatively. As shown in Fig. 1, compound **1** consists of one $[H_2W_{12}O_{40}]^{6-}$ unit, two lanthanum ions La^{3+}, four pyridine-4-carboxylate ligands (L), and eleven water molecules in the asymmetric unit. The bond valence sum calculations indicate that the La sites are in the +3 oxidation state and all W sites are in the +6 oxidation state [25]. The La^{3+} ion is in a distorted monocapped square antiprismatic geometry and is coordinated by one terminal oxygen atom of the $[H_2W_{12}O_{40}]^{6-}$ unit with a bond length of 2.483 Å, by five oxygen atoms of four pyridine-4-carboxylate ligands with an average bond length of 2.568 Å, and three aqua ligands with an average bond length of 2.525 Å. The pyridine-4-carboxylate ligands adopt two different coordination modes: bidentate bridging chelating (A) and

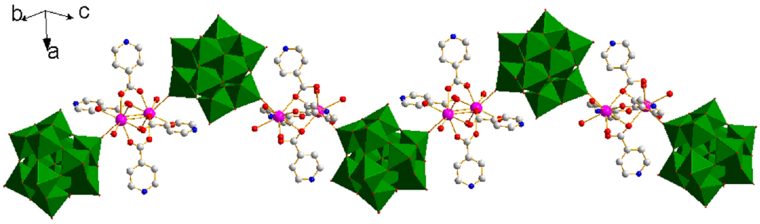

Fig. 3. View of the one-dimensional chain in **1** with hydrogen atoms omitted for clarity.

bidentate bridging (B). The modes A and B result in a dimeric La^{3+} coordination unit $\{(C_5H_5N\text{-}CO_2)_2La(H_2O)_3\}_2$ as shown in Fig. 2. Furthermore, the polyanion acts as a bidentate ligand and covalently binds to two $\{(C_5H_5N\text{-}CO_2)_2La(H_2O)_3\}_2$ units through two terminal oxygen atoms (O7 and O9), giving a 1D chainlike structure. The bond lengths are listed in Table 1. The variation of the La–O bond lengths results in the following sequence in the two compounds: La–O (H_2O) > La–Ot′ > La–O (L), which indicates that the electron-donating ability of the oxygen atoms is in the order of O (L) > Ot′ > O (H_2O) and that the La–O (L) bonds are stronger than the La–O (H_2O) or La–Ot′ bonds.

Interestingly, the polyanions $[H_2W_{12}O_{40}]^{6-}$ in compound **1** coordinate to the La^{3+} ions asymmetrically, rather than symmetrically *via* opposite oxygen atoms as reported for the compound $[\{Ce(NMP)_6\text{-}(PMo_{12}O_{40})\}]_n$ [26], so that the 1D chain is in a zigzag form (Fig. 3). Moreover, a 2D layer is formed *via* π–π stacking interactions with a distance of C(14)... C(17) of 3.471 Å (Fig. 4), and extensive hydrogen bonding interactions between adjacent chains in the 0 $\bar{1}$ 2 plane.

FT-IR spectroscopy

The spectra of the two compounds are very similar and therefore, the spectrum of compound **1** is described here representatively. The characteristic peaks at 1652, 1646, 1630, 1590, 1570, 1558 and 1403 cm^{-1} are indicative of the vibrations of the pyridine-4-carboxylate anions and water molecules. The peaks at 930, 880 and 781 cm^{-1} are attributed to the W=O and W–O–W unsymmetrical stretching vibrations, and the peak at 418 cm^{-1} to the La–O vibrations [27]. In comparison to the $[H_2W_{12}O_{40}]^{6-}$ clusters [28], compound **1** has similar peaks in the range 781 – 930 cm^{-1} except for slight shifts of some peaks due to the interaction between the polyanions and the La^{3+} cations in the solid state, which indicates that the polyanion in the title compound still retains the basic $[H_2W_{12}O_{40}]^{6-}$ structure. These results are consistent with those of the structural analysis.

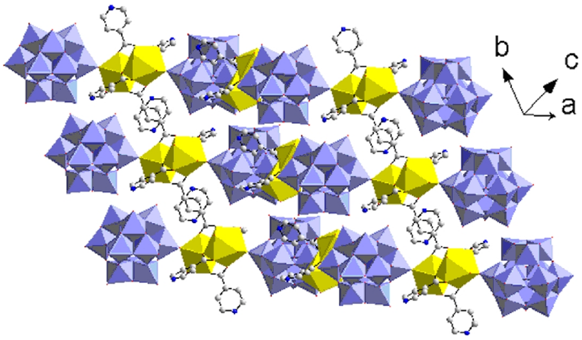

Fig. 4. View of the two dimensional-layer of polyhedra formed *via* π–π stacking interactions and extensive hydrogen-bonding interactions between chains in the 0 $\bar{1}$ 2 plane in compound **1**; all water molecules are omitted for clarity.

Thermal analysis

The TG curve of compound **1** is divided into two stages. The weight loss in the first stage is 5.68 % (calcd. 5.66 %) in the temperature range 0 – 499 °C, including two steps of water releases. The weight loss in the second stage is 12.88 % (calcd. 12.90 %) in the temperature range 571 – 668 °C, corresponding to the decomposition of organic components. The total weight loss (18.21 %) is in good agreement with the calculated value (18.56 %). The sample weight was unchanged at temperatures higher than 668 °C. The TG curve of compound **2** exhibits similar weight loss stages, the overall weight loss being 19.88 %, in agreement with the calculated value of 20.12 %, considered as the loss of all water and the decomposition of the organic moieties.

Cyclic voltammetry

To study the redox properties of compounds **1** and **2**, their CVs (0.1 mmol L^{-1}) were performed in a 0.5 mol L^{-1} Na_2SO_4 solution (pH = 3.11), and the

Compound	$(NH_4)_6[H_2W_{12}O_{40}]\cdot 3H_2O$		**1**		**2**	
E_{cp}, V	−0.744	−0.556	−0.708	−0.539	−0.700	−0.526
E_{ap}, V	−0.672	−0.493	−0.666	−0.489	−0.645	−0.482
ΔE_p, mV	72	63	42	50	55	44
$E_{1/2}$, V	−0.708	−0.524	−0.667	−0.514	−0.672	−0.504

Table 2. Cathodic (E_{cp}) and anodic (E_{ap}) peak potentials and potential differences for $(NH_4)_6[H_2W_{12}O_{40}]\cdot 3H_2O$, **1** and **2**.

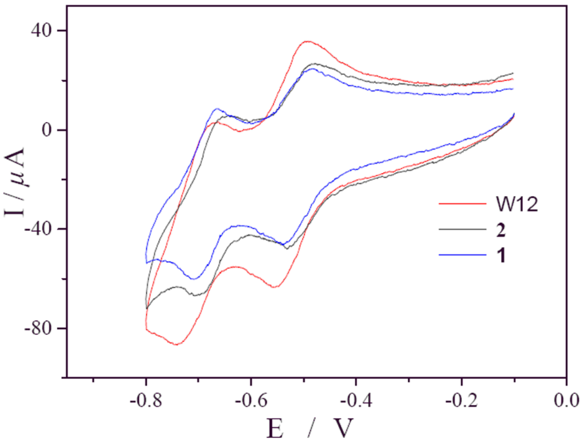

Fig. 5. Cyclic voltammograms of compounds $(NH_4)_6$-$[H_2W_{12}O_{40}]\cdot 3H_2O$ (W12), **1** and **2**.

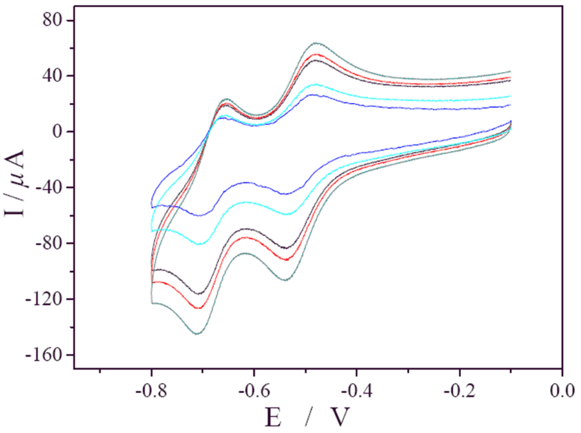

Fig. 6. The cyclic voltammograms of compound **2** at different scan rates (from inner to outer: 50, 80, 110, 140, and 170 mV s^{-1}).

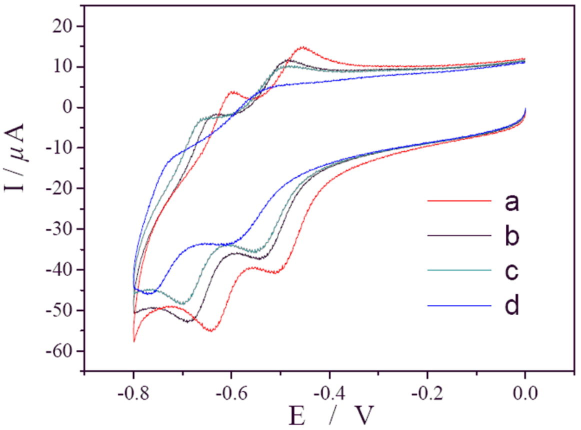

Fig. 7. The cyclic voltammograms of compound **2** in H_2SO_4+Na_2SO_4 aqueous solutions with different pH values (from outer to inner: 1.61, 2.16, 2.61 and 3.41).

CV of $(NH_4)_6[H_2W_{12}O_{40}]\cdot 3H_2O$ was also measured under identical conditions for comparison. From Fig. 5 it can be seen that the electrochemical properties of **1** and **2** are similar to that of the parent compound $(NH_4)_6[H_2W_{12}O_{40}]\cdot 3H_2O$, which undergoes a two-step two-electron redox process in the potential range 0 to −0.8 V. However, for **1** and **2**, the values of the mean peak potentials $E_{1/2} = (E_{ap} + E_{cp})/2$ are shifted in the positive direction as compared with their parent compound. The coordination interactions between the La^{3+}/Ce^{3+} complexes and the POMs anions in **1** and **2** may be responsible for these slight differences. Their peak potentials, $E_{1/2}$, and the peak-to-peak separations ($\Delta E_p = E_{ap} - E_{cp}$) are listed in Table 2. From Fig. 5 and the data in Table 2 it can be seen that the peak potentials for the two pairs of W redox peaks are hardly displaced, irrespective of whether the complex fragment is $[\{(C_5H_5N\text{-}CO_2)_2La(H_2O)_3\}_2]^{3+}$ or $[\{(C_5H_5N\text{-}CO_2)_2Ce(H_2O)_3\}_2]^{3+}$, which suggests that the $[H_2W_{12}O_{40}]^{6-}$ anions are the active centers for the hybrids' redox behavior.

Taking **2** as an example, the CV behavior at different scan rates was studied under the above-mentioned condition. As can be seen from Fig. 6, the anodic and cathodic peak currents increase gradually, and the peak potentials change gradually: the cathodic peak potentials shift in the negative direction and the corresponding anodic peak potentials move in the positive direction, with the scan rate varying from 50 to 170 mV s^{-1}. The peak-to-peak separation between the corresponding cathodic and anodic peaks increases with increasing scan rate, but the mean peak potentials do not change on the whole.

In addition, the pH of the supporting electrolyte solution has a marked effect on the electrochemical behavior of **2** in H_2SO_4+Na_2SO_4 aqueous solutions. It can be clearly seen in Fig. 7 that along with increasing pH, the anodic peak potentials and the corresponding cathodic potentials all gradually shift in the negative potential direction, and both the anodic and cathodic peak currents gradually decrease. Along with increasing pH, the lower concentration of protons in the solutions should be the reason for the current decrease, and the more negative reduction potentials can be elucidated by the Nernst equation [29].

Conclusions

In summary, we have synthesized two novel compounds, $[(C_5H_5N\text{-}CO_2)_2Ln(H_2O)_3]_2[H_2W_{12}O_{40}] \cdot nH_2O$ ($C_5H_5N\text{-}CO_2$ = pyridine-4-carboxylate; Ln = La^{3+} (**1**), n = 5; Ce^{3+} (**2**), n = 7), which represent the first 1D extended structures based on α-metatungstate anions and lanthanide ions together with organic anions. The isolation of compounds **1** and **2** shows a perspective of extending the POM family through selecting suitable lanthanide metals and organic ligands. Our results indicate that the α-metatungstate $[H_2W_{12}O_{40}]^{6-}$ cluster is a good candidate for designing new compounds with varying architectures and valuable properties. This work also paves the way for the assembly of α-metatungstate-based inorganic-organic hybrid materials containing other lanthanide ions.

Experimental Section

Chemicals and measurements

All chemicals were used as purchased without further purification. $(NH_4)_6[H_2W_{12}O_{40}] \cdot 3H_2O$ was synthesized according to the literature [30] and characterized by IR spectroscopy and TG analyses. Elemental analyses (C, H and N) were performed with a Perkin-Elmer 2400 CHN elemental analyzer and W, La and Ce were analyzed with a Leaman ICP atomic emission spectrometer. IR spectra were recorded in the range of 400 – 4000 cm^{-1} with an Alpha Centauri FT/IR spectrophotometer with KBr pellets. Cyclic voltammetry measurements were carried out with a CHI 660 electrochemical workstation using a conventional three-electrode single compartment cell at r. t. The working electrode was glassy carbon, the reference electrode was Ag/AgCl, the counter electrode was Pt gauze, and the scan rate was 100 mV/s. TG analyses were performed with a Perkin-Elmer TGA7 instrument in flowing N_2 with a heating rate of 10° min^{-1}.

Synthesis

$[(C_5H_5N\text{-}CO_2)_2La(H_2O)_3]_2[H_2W_{12}O_{40}] \cdot 5H_2O$ (1)

In a typical experiment, $(NH_4)_6[H_2W_{12}O_{40}] \cdot 3H_2O$ (0.0752 g, 0.025 mmol) was dissolved in water (8 mL). The pH value of the solution was carefully adjusted with a dilute NaOH solution (1 $mol \cdot L^{-1}$) to 7.68, and the solution was stirred for 10 min. A solution (8 mL) of $La(NO_3)_3 \cdot 6H_2O$ (0.0216 g, 0.050 mmol) was added and the mixture stirred for 10 min. Then pyridine-4-carboxylic acid (0.0123 g, 0.1 mmol) dissolved in hot water was added, and the resulting solution was stirred for 20 min at 60 °C. The filtrate was kept under ambient conditions. After 24 h colorless blocks of compound **1** were obtained. (yield 30 %, based on La). Anal. calcd. for **1**: C 7.55, H 1.16, N 1.47, W 57.80, La 7.28; found: C 7.58, H 1.18, N 1.46, W 57.60, La 7.21.

Table 3. Crystal data and structure refinement for **1** and **2**.

Complex	**1**	**2**
Empirical formula	$C_{24}H_{44}La_2N_4O_{59}W_{12}$	$C_{24}H_{48}Ce_2N_4O_{61}W_{12}$
Mr	3816.65	3855.07
Color, habit	colourless, block	yellow, block
Cryst. size, mm^3	$0.13 \times 0.13 \times 0.13$	$0.13 \times 0.13 \times 0.13$
Crystal system	triclinic	triclinic
Space group	$P\bar{1}$	$P\bar{1}$
a, Å	11.4720(6)	11.4925(9)
b, Å	11.4802(6)	11.5009(9)
c, Å	26.1102(13)	26.085(2)
α, deg	77.8250(10)	77.6010(10)
β, deg	87.8230(10)	87.6020(10)
γ, deg	89.7150(10)	89.6300(10)
V, $Å^3$	3358.9(3)	3364.4(5)
Z	2	2
D_{calcd}, g cm^{-3}	3.77	3.80
$\mu(MoK_\alpha)$, cm^{-1}	21.8	21.9
$F(000)$, e	3380	3416
hkl range	$-13 \le h \le 14$	$-14 \le h \le 13$
	$-14 \le k \le 12$	$-14 \le k \le 12$
	$-32 \le l \le 31$	$-30 \le l \le 32$
Refl. measured	17539	18788
Refl. unique	11974	12867
R_{int}	0.0415	0.0257
Ref. parameters	911	928
GoF (F^2)	1.041	1.116
$R(F)$	0.046	0.054
$wR(F^2)$ (all refl.)	0.105	0.106
$\Delta\rho_{fin}$ (max/min), e $Å^{-3}$	6.160/–1.844	4.672/–2.198

$[(C_5H_5N\text{-}CO_2)_2Ce(H_2O)_3]_2[H_2W_{12}O_{40}] \cdot 7H_2O$ (2)

This compound was prepared similar to **1**, with $Ce(NO_3)_3 \cdot 6H_2O$ instead of $La(NO_3)_3 \cdot 6H_2O$. Yellow blocks; yield 35 % based on Ce. Anal. calcd. for **2**: C 7.48, H 1.25, N 1.45, W 57.23, Ce 7.26; found: C 7.46, H 1.28, N 1.43, W 57.12, Ce 7.32.

X-Ray crystallograpphy

Diffraction data for **1** and **2** were collected with a Bruker Smart Apex CCD diffractometer with MoK_α radiation (λ = 0.71073 Å) at 194.5 K using the ω scan technique. Empirical absorption corrections were applied. The structures of **1** and **2** were solved by Direct Methods and refined by full-matrix least-squares on F^2 using the SHELX-97 software [31]. All non-hydrogen atoms were refined anisotropically and H atoms were placed in calculated positions. A summary of the crystallographic data and the numbers pertinent to the structure determination are provided in Table 3. Selected bond lengths and bond angles are listed in Table 1.

CCDC 622637 and 623483 contain the supplementary crystallographic data for this paper. These data can be obtained free of charge from the Cambridge Crystallographic Data Centre *via* www.ccdc.cam.ac.uk/data_request/cif.

Acknowledgement

This work was supported by the Analysis and Testing Foundation of the Northeast Normal University.

---

[1] M. T. Pope, *Heteropoly and Isopoly Oxometalates*; Springer, Berlin, **1983**.

[2] M. T. Pope, A. Müller, *Angew. Chem.* **1991**, *103*, 56 – 70; *Angew. Chem. Int. Ed.* **1991**, *30*, 34 – 38.

[3] *Polyoxometalates: From Platonic Solids to Anti-Retroviral Activity*, (Eds.: M. T. Pope, A. Müller), Kluwer Academic Publishers, Dordrecht, **1994**.

[4] M. T. Pope in *Comprehensive Coordination Chemistry II: From Biology to Nanotechnology*, Vol. 4, Ed.: A. G. Wedd, Elsevier, Oxford, **2004**, pp. 635 – 678.

[5] C. L. Hill in *Comprehensive Coordination Chemistry II: From Biology to Nanotechnology*, Vol. 4, Ed.: A. G. Wedd, Elsevier, Oxford, **2004**, pp. 679 – 759.

[6] Special issue: C. L. Hill (Ed.) *Chem. Rev.* **1998**, *98*, 1 – 2.

[7] Y. Xu, J. Q. Xu, K. L. Zhang, Y. Zhang, X. Z. You, *Chem. Commun.* **2000**, 153 – 154.

[8] a) P. J. Hagrman, D. Hagrman, J. Zubieta, *Angew. Chem.* **1999**, *111*, 2798 – 2848; *Angew. Chem. Int. Ed.* **1999**, *38*, 2638 – 2684; b) D. Hagrman, J. Zubieta, *Chem. Commun.* **1998**, 2005 – 2006; c) D. Hagrman, P. J. Hagrman, J. Zubieta, *Angew. Chem.* **1999**, *111*, 3359 – 3363; *Angew. Chem. Int. Ed.* **1999**, *38*, 3165 – 3168.

[9] X. Y. Wei, M. H. Dickman, M. T. Pope, *J. Am. Chem. Soc.* **1998**, *120*, 10254 – 10255.

[10] a) L. S. Felices, P. Vitoria, J. M. Gutiérrez-Zorrilla, S. Reinoso, P. Vitoria, L. Lezama, *Chem. Eur. J.* **2004**, *10*, 5138 – 5146; b) S. Reinoso, P. Vitoria, J. M. Gutiérrez-Zorrilla, L. Lezama, J. I. Beitia, *Inorg. Chem.* **2005**, *44*, 9731 – 9742.

[11] a) Y. P. Ren, X. J. Kong, X. Y. Hu, M. Sun, L. S. Long, *Inorg. Chem.* **2006**, *45*, 4016 – 4025; b) Y. P. Ren, X. J. Kong, L. S. Long, R. B. Huang, L. S. Zheng, *Cryst. Growth Des.* **2006**, *6*, 572 – 576.

[12] M. Yuan, Y. G. Li, E. B. Wang, C. G. Tian, L. Wang, C. W. Hu, *Inorg. Chem.* **2003**, *42*, 3670 – 3676.

[13] X. L. Wang, C. Qin, E. B. Wang, Z. M. Su, Y. G. Li, L. Xu, *Angew. Chem.* **2006**, *118*, 7571 – 7574; *Angew. Chem. Int. Ed.* **2006**, *45*, 7411 – 7414.

[14] H. Y. An, D. R. Xiao, E. B. Wang, Y. G. Li, Z. M. Su, L. Xu, *Angew. Chem.* **2006**, *118*, 918 – 922; *Angew. Chem. Int. Ed*, **2006**, *45*, 904 – 908.

[15] L. Xu, H. Zhang, E. Wang, D. G. Kurth, Z. Li, *J. Mater. Chem.* **2002**, 654 – 657.

[16] C. Benelli, D. Gatteschi, *Chem. Rev.* **2002**, *102*, 2369 – 2388.

[17] T. Yamase, *Chem. Rev.* **1998**, *98*, 307 – 326.

[18] C. D. Wu, C. Z. Lu, H. H. Zhuang, J. S. Huang, *J. Am. Chem. Soc.* **2002**, *124*, 3836 – 3837.

[19] a) H. Zhang, L. Y. Duan, Y. Lan, E. B. Wang, C. W. Hu, *Inorg. Chem.* **2003**, *42*, 8053 – 8058; b) X. L. Wang, Y. Q. Guo, Y. G. Li, E. B. Wang, C. W. Hu, N. H. Hu, *Inorg. Chem.* **2003**, *42*, 4135 – 4140; c) R. C. Howell, F. G. Perez, S. Jain, W. D. Horrocks, A. L. Rheingold, L. C. Francesconi, *Angew. Chem.* **2001**, *113*, 4155 – 4158; *Angew. Chem. Int. Ed.* **2001**, *40*, 4031 – 4034.

[20] a) X. Fang, T. M. Anderson, W. A. Neiwert, C. L. Hill, *Inorg. Chem.* **2003**, *42*, 8600 – 8602; b) M. Sadakane, M. H. Dickman, M. T. Pope, *Angew. Chem.* **2000**, *112*, 3036 – 3038; *Angew. Chem. Int. Ed.* **2000**, *39*, 2914 – 2916; c) K. Wassermann, M. T. Pope, *Inorg. Chem.* **2001**, *40*, 2763 – 2768; d) K. Fukaya, T. Yamase, *Angew. Chem.* **2003**, *115*, 678 – 682; *Angew. Chem. Int. Ed.* **2003**, *42*, 654 – 658.

[21] a) Y. Lu, Y. Xu, Y. G. Li, E. B. Wang, X. X. Xu, Y. Ma, *Inorg. Chem.* **2006**, *45*, 2055 – 2060; b) C. Zhang, R. C. Howell, Q. H. Luo, H. L. Fieselmann, L. J. Todaro, L. C. Francesconi, *Inorg. Chem.* **2005**, *44*, 3569 – 3578.

[22] a) H. Y. An, Y. G. Li, D. R. Xiao, E. B. Wang, C. Y. Sun, *Cryst. Growth Des.* **2006**, *6*, 1107 – 1112; b) H. Y. An, D. R. Xiao, E. B. Wang, Y. G. Li, L. Xu, *New. J. Chem.* **2005**, *29*, 667 – 672.

[23] X. T. Zhang, D. Q. Wang, J. M. Dou, S. S. Yan, X. X. Yao, J. Z. Jiang, *Inorg. Chem.* **2006**, *45*, 10629 – 10635.

[24] a) C. R. Sprangers, J. K. Marmon, D. C. Duncan, *Inorg. Chem.* **2006**, *45*, 9628 – 9630; b) D. L. Long, H. Abbas, P. Kogerler, L. Cronin, *J. Am. Chem. Soc.* **2004**, *126*, 13880 – 13881; c) R. N. Devi, E. Burkholder, J. Zubieta, *Inorg. Chim. Acta* **2003**, *348*, 150 – 156.

[25] I. D. Brown, D. Altermatt, *Acta Crystallogr.* **1985**, *41B*, 244 – 247.

[26] J. Y. Niu, M. L. Wei, J. P. Wang, D. B. Dang, *Eur. J. Inorg. Chem.* **2004**, 160 – 170.

[27] a) M. Fournier, R. Thouvenot, C. Rocchiccioli-Deltcheff, *J. Chem. Soc., Faraday Trans.* **1991**, *87*,

349 – 356; b) K. Nomiya, R. Kobayashi, M. Miwa, *Bull. Chem. Soc. Jpn.* **1983**, *56*, 2272 – 2275.

[28] J. H. Son, Y. U. Kwon, *Inorg. Chim. Acta* **2005**, *358*, 310 – 314.

[29] a) J. Wang, *Analytical Electrochemistry*, VCH, New York, **1994**; b) C. M. A. Brett, A. M. O. Brett, *Electrochemistry, Principles, Methods and Applications*, Chapter. 2, Oxford University Press, Oxford, **1993**.

[30] J. H. Son, Y. U. Kwon, O. H. Han, *Inorg. Chem.* **2003**, *42*, 4153 – 4159.

[31] G. M. Sheldrick, SHELXS/L-97, Programs for Crystal Structure Determination, University of Göttingen, Göttingen (Germany) **1997**.